united nations
educational, scientific
and cultural
organization

international atomic
energy agency

the
**abdus salam**
international centre for theoretical physics

SMR 1161/32

## AUTUMN COLLEGE ON PLASMA PHYSICS

25 October - 19 November 1999

# MHD Waves in Solar Coronal Structures

V.M. NAKARIAKOV

University of Warwick
U.K.

# Magnetohydrodynamic (MHD) Waves in Solar Coronal Structures

Valery M. Nakariakov

University of Warwick

UK.

"Busy old fool, unruly Sun, Why dost thou thus?"
- John Donne (1572-1631) "The Sun Rising"

# 1 Introduction

## 1.1 What is the solar corona and why do we study it?

The corona of the Sun is the upper, hottest and magnetically dominated part of the solar atmosphere.

Main physical facts about the corona:

- Temperature is over 1 MK (c.f. $T_{\text{photosphere}} \leq 6000$ K.
- Plasma is mainly hydrogen and is almost fully ionized, $n = 5 \times 10^{14}$ m$^{-3}$.
- Plasma-$\beta$ (ratio of kinetic and magnetic pressures) is low (0.001-0.01). The plasma is "cold"!
- Plasma is gravitationally stratified, the scale height $H$ is about 50-60 Mm (c.f. $R_\odot = 696$ Mm).
- The origin of the solar wind. (Speeds are up to several hundred km/s at a few $R_\odot$).

Fundamental puzzles of the corona:

- What mechanisms are responsible for heating of the corona up to several million K?
- What accelerates the solar wind up to measured speeds exceeding 700 km/s?
- What are the physical processes behind solar flares and coronal mass ejections, magnificent phenomena accompanied by an enormous energy release?

## 1.2 How do we study the corona?

Historically, first observations of the corona were taken during total solar eclipses. But, the eclipses are rare and last not longer than several minutes.

Main information on dynamical phenomena in the corona come from space-based UV, EUV and X-ray telescopes. Now, there are SOHO, Yohkoh and TRACE missions operating in space, which provide us with incredibly high resolution data in these bands.

| Instrument | Spatial Res. | Temporal res. | Band | |
|---|---|---|---|---|
| SOHO: | | | | |
| EIT | $\leq$ 1" | $\geq$ 50 s | EUV | images |
| CDS | 1"×2" | few s | EUV | |
| UVCS | 12" – 5' | s – h | UV-EUV,WL | |
| LASCO-C1 | 5.6" | 60 s | WL | |
| C2 | 11.4" | | | |
| C3 | 56.0" | | | |
| SUMER | 1.2–1.5" | $\geq$30 s | EUV | |
| Yohkoh | 4" (SXT) | few s | SX, HX | |
| TRACE | 0.5" | 30 s | UV-EUV, WL | images |
| SPARTAN-201 | 22.5" | 1-15 s (WL) | UV-EUV,WL | |

(1"$\approx$730 km)

Also, we can observe the coronal plasma in the radio band and by interplanetary scintillation.

## 1.3 Structures in the corona

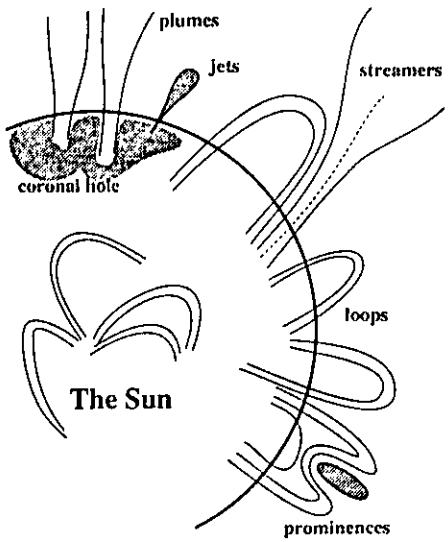


The corona is highly structured:

- Open structures: coronal holes, streamers, plumes inside the holes.

- Closed structures: loops ($R$ up to 100-200 Mm).

In addition, there are plasma jets of various scales and speeds, prominences, etc.

## 1.4 Why do we study waves in the corona?

Coronal waves are associated with

1. development of plasma perturbations,
2. transfer of energy and momentum,
3. coronal heating / solar wind acceleration,
4. coronal seismology.

Also, because they are there!

# 2 Do we see waves in the corona?

MHD waves and oscillations have been observed for a long time in radio and optic bands:

Prominence oscillations

> Periodic velocity and intensity oscillations with various periods: e.g. 1 hour, 3–5 min, 30 s. (They are seen from the Earth).
>
> (E.g. IAU colloquium 117, 1990)

Radio pulsations (e.g. Aschwanden 1987 for a review).

> Roberts, Edwin and Benz 1983: Type IV radio events as fast waves trapped in loops. The idea of *coronal seismology.*

EUV oscillations

> Chapman et al. 1972 using GSFC extreme-ultraviolet spectroheliograph on OSO-7 (spatial resolution was $10 \times 20$ arcsec, cadence time was 5.14 s) have found Mg VII, Mg IX and He II emission intensity periodicities at about 262 s.

Antonucci et al. 1984 using Harvard College Observatory EUV spectroheliometer on Skylab have detected oscillations in the C II, O IV, and Mg X emission intensity with periods of 117 s and 141 s.

Soft X-ray oscillations

Harrison 1987 with Hard X-ray Imaging Spectrometer on SMM have detected soft X-ray (3.5-5.5 keV) pulsations of period 24 min (for six hours).

Very recently, new types of large scale wave motions have been discovered in the corona:

- **Compressive waves in polar plumes**
  *DeForest & Gurman 1998; Ofman, Nakariakov and DeForest 1999:* SOHO/EIT and TRACE:

  Outwardly propagating perturbations of the intensity (plasma density) at 1.01–1.2 $R_\odot$,

  Quasiperiodic groups of 3-10 periods,

  Periods about 10-15 min,

  The duty cycle is roughly balanced,

  $V_{\rm phase} \approx 75 - 150$ km/s,

  Amplitude $\approx 2 - 4$ % and growing with height).

  *Ofman et al. 1997*, white light channel (WLC) of the SOHO/UVCS: density fluctuations with periods $\approx 9$ min at $1.9R_\odot$ in coronal holes.

- **Compressive waves in long loops**
  *Berghmans & Clette 1999, using SOHO/EIT and TRACE:*

  Upwardly propagating perturbations of the intensity (plasma density) (very similar to the previous case, but on the disc),

  With speed about 65–165 km/s,

  Amplitude is $\approx 2\%$ in intensity ($\approx 2$ % in density),

The heigh growth of the amplitude has not been found,

No manifestation of downward propagation.

Traveling along almost all loops analyzed.

- **Coronal Moreton waves**
  *Thompson et al. 1999:* SOHO/EIT

  Properties accumulated from observations of more than 50 events.
  (see *http://umbra.nascom.nasa.gov/bjt/lscd/* for details)

  They prefer to propagate radially, stopping at neutral lines and coronal hole boundaries, and distorted by active regions.

  Speeds range from 200-600 km/sec.

  Active regions distort the waves locally, bending them toward the lower Alfvén speed regions

  They can cause "visible deflection" of coronal magnetic field lines and probably are associated with filament oscillations (such as "Flare-Initiated Filament Oscillations" Ramsey, H.E. and Smith, S.F., 1966 Astron. J. 71, 197-199).

  Propagating regions usually consist of only an increase in emission for a single frame. The detectable change in emission can extend far into the corona (1.5 solar radii).

  The waves do not show observable signs of propagation into coronal holes. This may be due to depleted emission in coronal holes, or due to an increase of wave speed and subsequent decrease in amplitude, or both.

  "Twin" events from the same region show similar propagation paths.

  Can cause activity at the coronal hole boundaries - what appears to be a widening or closing along a hole may also be attributed to a change in obscuration by coronal field lines.

  Usually associated with SOHO/LASCO white light observations of Coronal Mass Ejections (CME).

  Speed, intensity of emission, speed, x-ray signature have no apparent correlation.

- **Post-flare oscillation of loops**
  *Nakariakov et al. 1999, Aschwanden et al. 1999, TRACE*

  Decaying kink-like oscillations of coronal loops, excited by a nearby flare.
  (By a coronal Moreton wave?)

  Periods are several minutes (e.g 256 s),

  Displacement amplitudes are about several Mm for loop radii about 100 Mm,

  Decay time about 14.5 min.

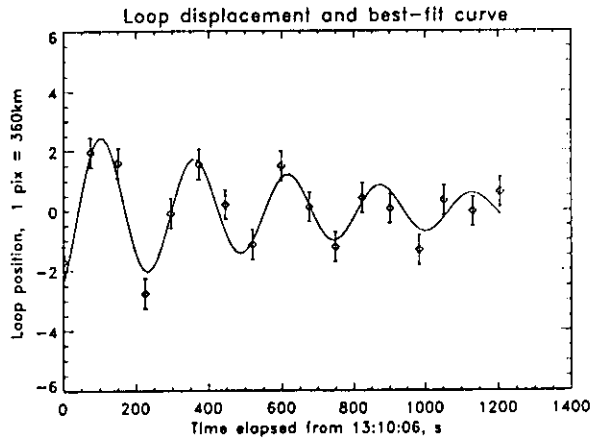


- **Non-thermal broadening of coronal emission lines.**

  (Most probably associated with MHD waves).

  *Ofman & Davila 1997* using SOHO UVCS:
  up to 300 km/s unresolved motions at about 1.7 $R_\odot$.

  *Banerjee et al. 1998* using SOHO SUMER:
  non-thermal line-of-sight (LOS) velocity increases from 27 km/s at 20 Mm above the limb to 46 km/s at 62 Mm.

  *Chae et al. 1998* using SOHO SUMER:
  LOS velocities of 20-30 km/s on the disc.

  SPARTAN-201
  LOS velocities up to 20-30 km/s.

*Esser et al. 1999* using SOHO UVCS:
LOS velocities of 20-23 km/s at 1.35-2.1 $R_\odot$

- **Tornados.**

  (May be connected with MHD waves). *Pike & Mason 1998*, SOHO CDS:

  Macrospicule-like (a jet) features have now been identified in the polar regions both on the limb and disk. These show blue- and red-Doppler-shifted emission on either side of the feature axis. Indication of the presence of a rotation (a solar tornado). The rotation velocities ($\approx$ 150 $km/s$) increase with height.

# 3 What are MHD waves?

## 3.1 Governing equations and assumptions

MHD waves are propagating perturbations of magnetic field and plasma velocity and plasma mass density, described by the MHD (single fluid approximation) set of equations, which connects the magnetic field B, plasma velocity V, kinetic pressure $p$ and density $\rho$ through the equations:

$$\rho\frac{\partial \mathrm{V}}{\partial t} + \rho(\mathrm{V}\cdot\nabla)\mathrm{V} = -\mathrm{grad}p - \frac{1}{4\pi}\mathrm{B}\times\mathrm{curl}\ \mathrm{B} + \mathcal{F}, \tag{1}$$

$$\frac{\partial \mathrm{B}}{\partial t} = \mathrm{curl}[\mathrm{V}\times\mathrm{B}], \tag{2}$$

$$\frac{\partial \rho}{\partial t} + \mathrm{div}(\mathrm{V}\rho) = 0, \tag{3}$$

$$\frac{d}{dt}\left(\frac{p}{\rho^\gamma}\right) = 0, \tag{4}$$

which are the Euler, induction, continuity and adiabatic equations, respectively. The term $\mathcal{F}$ is an external force acting on a unit of volume of the plasma, for example, the gravity, $\mathcal{F} = -\mathrm{g}\rho$, where g is the gravity acceleration. Sometimes, it is convenient to supply set (1)-(4) by the equation

divB = 0, although this condition is implicitly contained in the Euler equation.

The applicability conditions are:

1. Speeds are much less than the speed of light. (in the solar corona: $V <$ a few thousand km/s)

2. Characteristic times are much longer than the Larmor rotation period and the plasma period.
   In the solar corona: $f_{MHD} < 1$ Hz
   with $f_{\rm gyro} = 1.52 \times 10^3 \times B({\rm G}) \approx 1.52 \times 10^4$ Hz
   and $f_{\rm plasma} = 9 \times n_e^{1/2}({\rm m}^{-3}) \approx 2 \times 10^8$ Hz,
   (for $B = 10$ G and $n_e = 5 \times 10^{14}$ m$^{-3}$).

3. Characteristic times are much longer than the collision times.

4. The Hall effect is insignificant:

$$\mathcal{H} = \frac{2\pi C_A}{\omega_{gyro}\lambda} \approx \frac{5 \times 10^2}{\lambda({\rm m})}. \tag{5}$$

   (e.g., for $\lambda = 5 \times 10^5$ m, $\mathcal{H} = 0.001$, )

## 3.2 Linear MHD waves in homogeneous media

Consider perturbation propagating along the $z$-axis. The straight and homogeneous magnetic field is in the $xz$-plane and has two components:

$$\mathbf{B_0} = B_0 \sin\alpha\,\mathbf{x_0} + B_0 \cos\alpha\,\mathbf{z_0}, \tag{6}$$

where $B_0$ is the absolute value of the magnetic field, $\alpha$ is the angle between the magnetic field and $z$-axis:

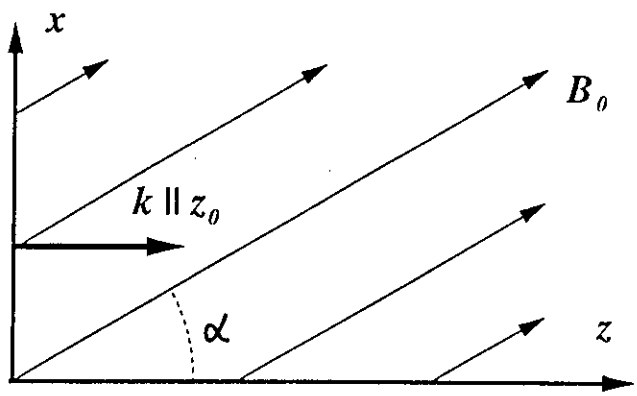


Characteristic speeds: the Alfvén speed $C_A = B_0(4\pi\rho_0)^{-1}$, the sound speed $C_s = (\gamma p_0/\rho_0)^{1/2}$.

In this geometry, in the linear limit, the MHD set of equation (1)-(4) splits into two uncoupled partial subsets, for the variables $V_y$ and $B_y$, and for $\rho$, $p$, $V_x$, $V_z$ and $B_x$. The first set describes the Alfvén wave, and can be reduced to the wave equation

$$\left(\frac{\partial^2}{\partial t^2} - C_{Az}^2 \frac{\partial^2}{\partial z^2}\right) V_y = 0, \tag{7}$$

where $C_{Az} = B_0 \cos\alpha/(4\pi\rho_0)^{1/2}$. The Alfvén wave does not perturb the density $\rho$ and, consequently, is incompressible (in the linear limit).

When $\mathbf{B_0}||\mathbf{z_0}$ there can be two *linearly polarized* Alfvén waves, $V_y$, $B_y$ and $V_x$, $B_x$.

Their combination can give us *elliptically polarized* Alfvén waves:

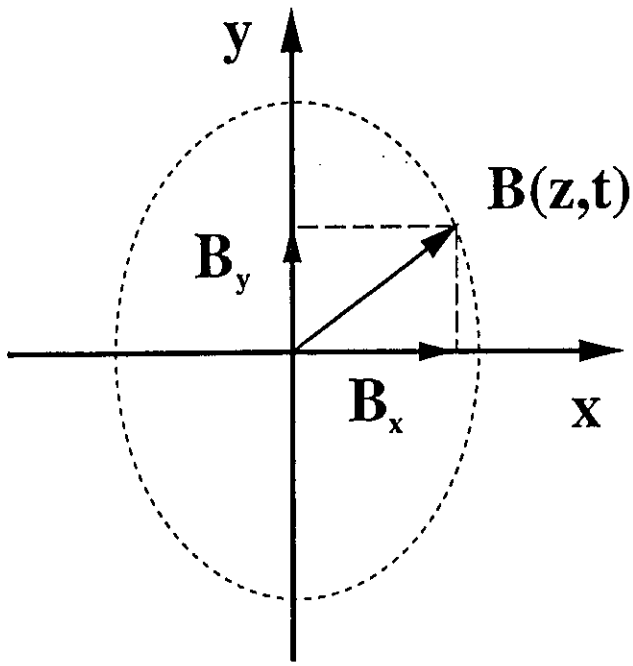


When $B_x^{\max} = B_y^{\max}$, the wave is *circularly polarized*, with $|B| = \text{const}$.

The circularly polarized Alfvén waves (even of finite amplitude) are *exact* solution of ideal MHD equations for an homogeneous medium.

The second set of equations describes magnetoacoustic waves and reduces to the equation

$$\left[\left(\frac{\partial^2}{\partial t^2} - C_{Az}^2\frac{\partial^2}{\partial z^2}\right)\left(\frac{\partial^2}{\partial t^2} - C_s^2\frac{\partial^2}{\partial z^2}\right) - C_{Ax}^2\frac{\partial^4 V_z}{\partial z^2 \partial t^2}\right] V_z = 0, \qquad (8)$$

where $C_{Azx} = B_0 \sin\alpha/(4\pi\rho_0)^{1/2}$. Supposing $V_z \sim \exp(i\omega t - ikz)$, we obtain the dispersion relation for the magnetosonic waves from Eq. (8):

$$(\omega^2 - C_A^2\cos^2\alpha\, k^2)(\omega^2 - C_s^2k^2) - C_A^2\sin^2\alpha\omega^2k^2 = 0. \qquad (9)$$

There are two magnetoacoustic modes, *fast* and *slow*, with quite different properties.

Polar plot for phase speeds $(\omega/k)$ for $\beta < 1$:

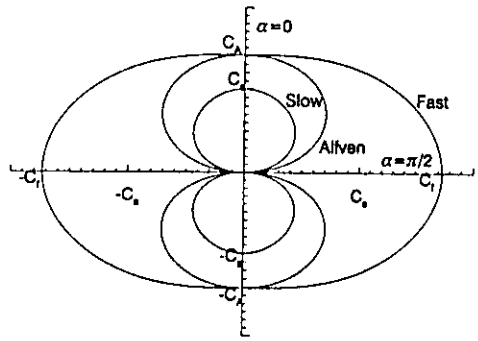


Polar plot for group speeds ($\mathrm{d}\omega/\mathrm{d}k$):

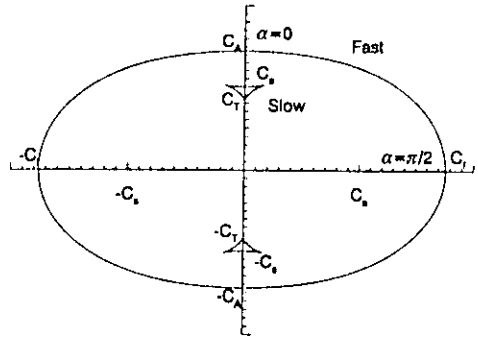


Alfvén waves propagate *strictly* along the magnetic field.
Slow waves are also confined to the magnetic field.
Fast wave propagation is almost isotropic.

# 4 MHD waves in coronal structures. Theoretical aspects.

Consider a static one-dimensional plasma inhomogeneity, described by $\rho_0$, $p_0$, and $B_0\mathbf{e}_z$ which are functions of the transversal coordinate $x$. The magnetic field lines are straight.

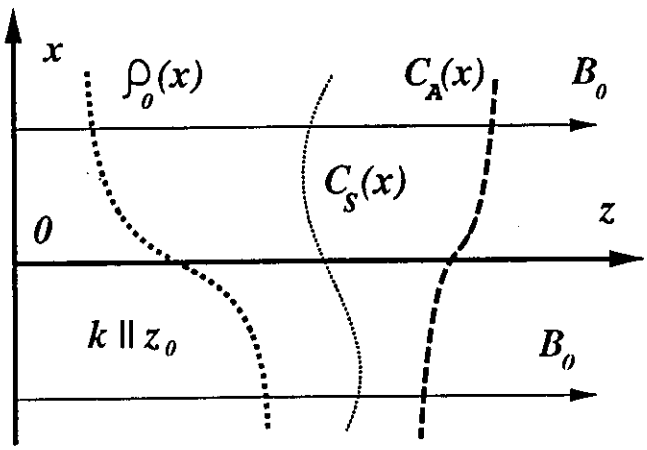


Total pressure balance has to be preserved everywhere,

$$p_{\rm total}(x) = p_0(x) + \frac{B_0^2(x)}{8\pi} = \text{const.} \tag{10}$$

Such a structure is called a *magnetic slab.*

Characteristic speeds: the Alfvén speed

$$C_A(x) = \frac{B_0(x)}{4\pi\rho_0(x)}^{1/2}, \tag{11}$$

the sound speed

$$C_s(x) = (\gamma p_0/\rho_0)^{1/2} \tag{12}$$

and the tube (or "cusp") speed

$$C_T = \frac{C_s C_A}{(C_s^2 + C_A^2)^{1/2}}. \tag{13}$$

Consider perturbation as $\Psi(x)\exp(i\omega t - ik_y y - ik_z z)$ + Boundary conditions in $x$,
aiming to get the dispersion relations

$$\mathcal{D}(\omega, k_y, k_z, [B_0(x), \rho_0(x) \text{ and } p_0(x)]) = 0. \tag{14}$$

Considering processes in the plane ($x, z$ only, $\partial/\partial y = 0$, but $V_y$, $B_y \neq 0$ (2.5D approximation), we have two linearly decoupled sets of MHD modes: Alfvén waves ($V_y, B_y \neq 0$), described by

$$\left[\omega^2 - C_A^2(x)k_z^2\right] V_y = 0. \qquad (15)$$

and magnetoacoustic (modified slow and fast magnetoacoustic waves) ($V_x, V_z, B_x, B_z, \rho \neq 0$), described by

$$\frac{d}{dx}\left[\frac{\varepsilon(x)}{m_0^2(x)}\frac{dV_x}{dx}\right] - \epsilon(x)V_x = 0, \qquad (16)$$

where

$$\varepsilon(x) = \rho_0(x)\left[\omega^2 - k_z^2 C_A^2(x)\right],$$

$$m_0^2(x) = \frac{(k_z^2C_s^2 - \omega^2)(k_z^2C_A^2 - \omega^2)}{(C_s^2 + C_A^2)(k_z^2C_T^2 - \omega^2)}.$$

+ appropriate boundary conditions

$\Rightarrow$ an eigenvalue problem.

The eigenfunctions gives us the transversal (in the $x$ direction) structure of the waves and eigenvalues define dispersion of the waves.

An exact analytical solution of the eigenvalue problem can be found just for a few transversal profiles of the stationary values $B_0(x)$, $\rho_0(x)$ and $p_0(x)$.

In a general case, equation (16) can have two singularities defined by conditions $\varepsilon(x) = 0$ and $m_0^{-1}(x) = 0$. The singularities take place at the Alfvén resonant layer where $\omega/k_z = C_A(x)$, and cusp resonant layer at $\omega/k_z = C_T(x)$.

## 4.1 Magnetoacoustic modes.

Equation (16) can have solutions, evanescent at the infinity, called *modes* or *trapped* or *guided* (or *ducted*) waves. The modes are *dispersive*.

Dispersion is determined by the ratio of the longitudinal wavelength to the characteristic spatial scale of inhomogeneity.

The modes can have different structures in $x$ direction, which allows us to classify them. For a localized inhomogeneity ($dB_0(x)/dx$, $d\rho_0(x)/dx$ and $dp_0/dx$ tend to zero for $|x| \to \infty$) with even profiles of $B_0(x)$, $\rho_0(x)$ and

$p_0(x)$, we can distinguish between *kink* and *sausage* modes (perturbing or not perturbing the structure axis, respectively),

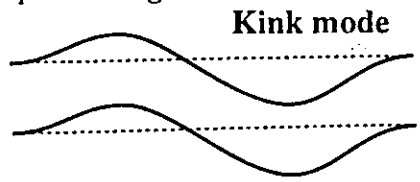


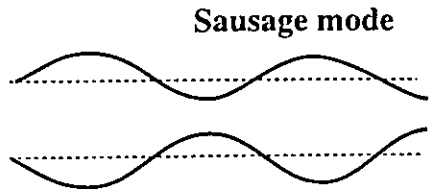


and between *body* and *surface* modes (oscillating or evanescent inside the structure, respectively).

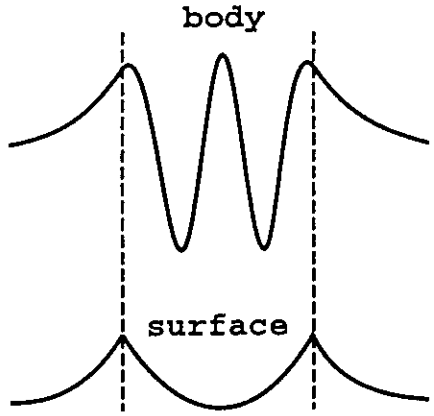


In addition, different modes of the same parity and transversal structure can be distinguished as *slow* and *fast* modes.

## 4.2 Magnetic flux tubes and slabs.

Two most developed models of the inhomogeneity are *magnetic flux slab* and *tube*. Consider a tube of a uniform plasma of the density $\rho_0$ and pressure $p_0$, penetrated by the magnetic field $\mathbf{B} = B_0\mathbf{e_z}$ and confined to $r < a$ by an external gas pressure $p_e$ and the magnetic field $\mathbf{B} = B_e\mathbf{e_z}$. The external

plasma is of the density $\rho_e$. So,

$$B_0(r) = \begin{cases} B_0, & r < a, \\ B_e, & r > a, \end{cases} \qquad \rho_0(r) = \begin{cases} \rho_0, & r < a, \\ \rho_e, & r > a. \end{cases} \tag{17}$$

Tube geometry:

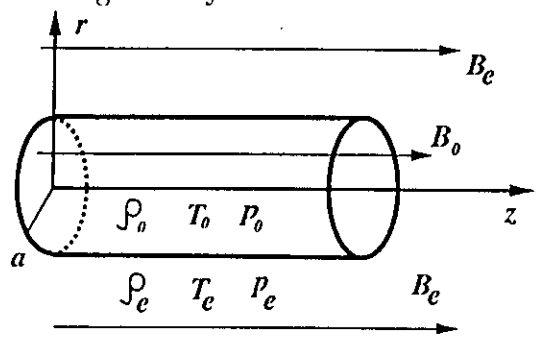


Slab geometry:

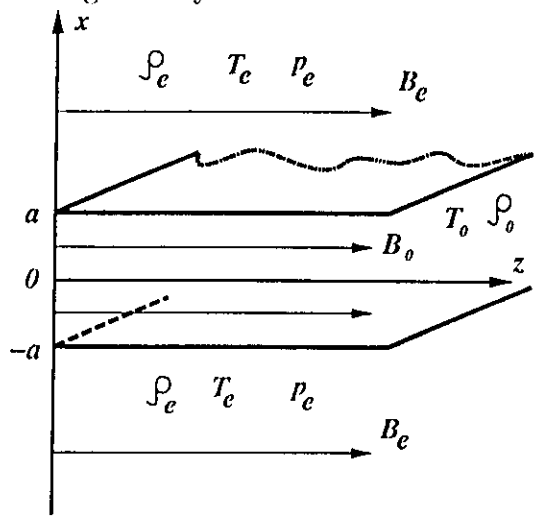


The sound speeds are $C_{s0}$ and $C_{se}$, Alfvén speeds $C_{A0}$ and $C_{Ae}$ and tube speeds $C_{T0}$ and $C_{Te}$ in the internal and external media, respectively.

At the boundary $r = a$ ($x = \pm a$):

$$p_0 + B_0^2/8\pi = p_e + B_e^2/8\pi. \tag{18}$$

External and internal solutions of the MHD equations have to be matched by the boundary conditions:

$$p_{\text{total}}^{\text{internal}}(r = a) = p_{\text{total}}^{\text{external}}(r = a) \tag{19}$$

and

$$V_x^{\text{internal}}(r=a) = V_x^{\text{external}}(r=a) \tag{20}$$

and

$$V_x^{\text{external}}(r \to \infty) \to 0 \tag{21}$$

(Note, that, in the presence of a steady flow, condition (20) has to be replaced by the continuity of the transversal displacement.)

Similar boundary conditions are in the slab case.

The dispersion relation is

$$\rho_e(\omega^2 - k_z^2 C_{Ae}^2) m_0 \frac{I_n'(m_0 a)}{I_n(m_0 a)} + \rho_0(k_z^2 C_{A0}^2 - \omega^2) m_e \frac{K_n'(m_0 a)}{K_n(m_0 a)} = 0, \tag{22}$$

where

$$m_\alpha^2 = \frac{(k_z^2 C_{s\alpha}^2 - \omega^2)(k_z^2 C_{A\alpha}^2 - \omega^2)}{(C_{s\alpha}^2 + C_{A\alpha}^2)(k_z^2 C_{T\alpha}^2 - \omega^2)}, \tag{23}$$

with $\alpha = 0, e$; $I_n(x)$ and $K_n(x)$ are modified Bessel functions of order $n$; the prime denotes the derivative of a function with respect to its argument. For the trapped modes, the condition $m_e > 0$ has to be fulfilled. The number $n$ determines the mode structure:

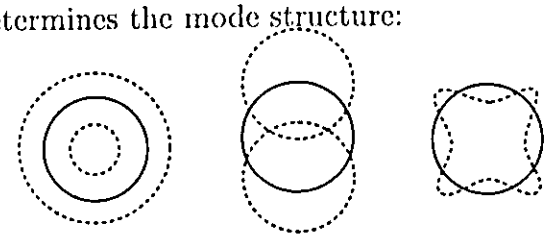


The similar dispersion relation for the magnetic slab is

$$\rho_e(k_z^2 C_{Ae}^2 - \omega^2) m_0 \left\{ \begin{array}{c} \tanh \\ \coth \end{array} \right\} m_0 a + \rho_0(k_z^2 C_{A0}^2 - \omega^2) m_e = 0, \tag{24}$$

where $a$ is the slab semi-width and the tanh/coth terms correspond to the sausage/kink modes.

Equations (22) and (24) describe both surface (for $m_0^2 > 0$) and sausage ($m_0^2 < 0$) modes. The strongest dispersion takes place for waves with lengths about the characteristic length $a$.

Typical examples. Dispersion curves for a coronal magnetic flux tube ($\beta \ll 1$, the slab geometry):

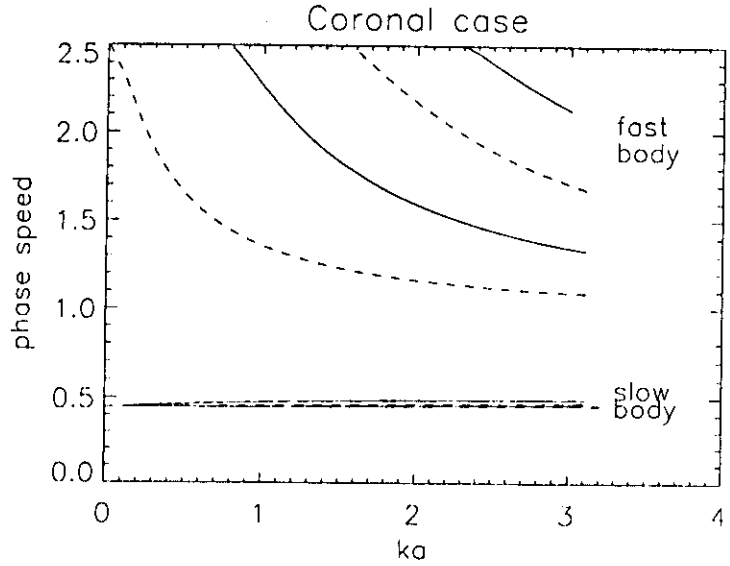


Dispersion curves for photospheric magnetic flux tube ($\beta \approx 1$, the slab geometry):

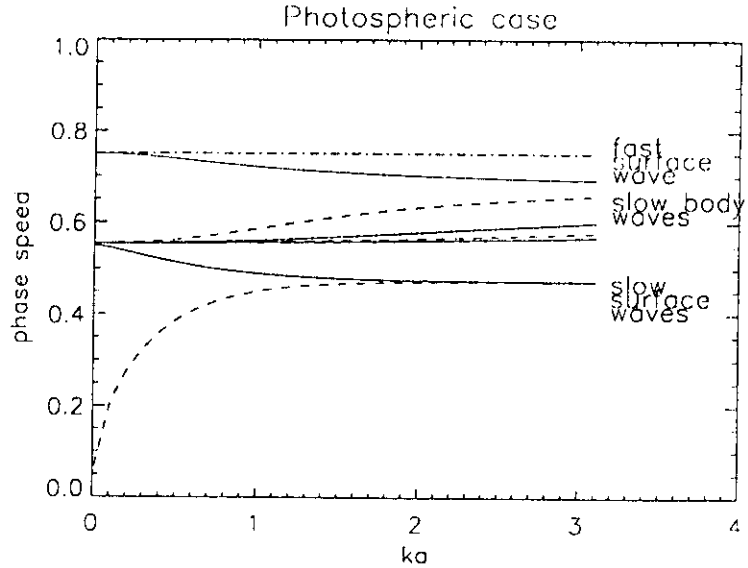

## 4.3 Refractive fast magnetoacoustic waveguides.

When $C_s \ll C_A$ ($\beta \ll 1$, which is typical for the corona), we can put $C_s = 0$ and significantly simplify description of fast magnetoacoustic waves. Equation (16) reduces to

$$\frac{d^2 V_x}{dx^2} + \left( \frac{\omega^2}{C_A^2(x)} - k^2 \right) V_x = 0; ) \tag{25}$$

$$V_x(x \to \pm\infty) = 0; \tag{26}$$

The eigenfunctions $V_x(x)$ define the transversal structure of the inhomogeneity modes. The corresponding eigenvalues connect $\omega$ and $k$ through dispersion relations.

Equations (25) mathematically identifies the quantum mechanical problem of determining a particle's behaviour in a potential well (the stationary Schrödinger equation).

The inhomogeneity considered guides fast magnetoacoustic waves in the neighbourhood of a *minimum* in the Alfvén speed, corresponding to a *maximum* in the plasma density in low-$\beta$ plasma.

For several special profiles of $\rho_0(x)$, the eigenvalue problem (25), (26) can be solved analytically.

A convenient profile of $\rho_0(x)$ has been suggested by Nakariakov & Roberts (1995b)

$$\rho(x) = \rho_\infty + (\rho_0 - \rho_\infty)\mathrm{sech}^2[(|x|/d)^p], \qquad p \geq 0, \tag{27}$$

which gives a smoothly varying density structure, varying from $\rho_0$ at $x = 0$ to $\rho_\infty$ as $|x| \to \infty$. For arbitrary power $p$, eigenvalue problem (25)-(26) requires a numerical solution. The profile (27) is of interest because it possesses two analytically solvable limiting cases: $p \to \infty$ and $p = 1$, which are the cases of the step profile and symmetric Epstein profile, respectively.

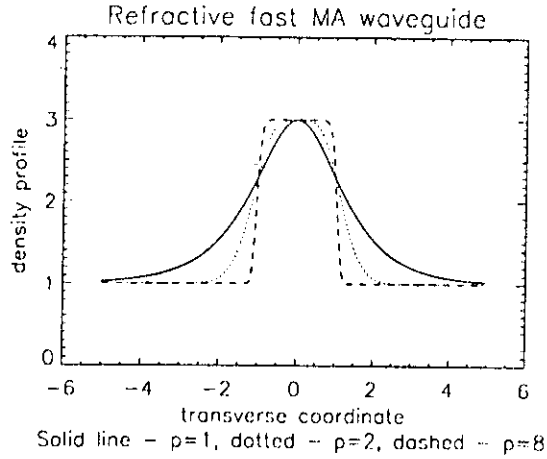


A typical dispersion diagram for a refractive fast magnetoacoustic waveguide:

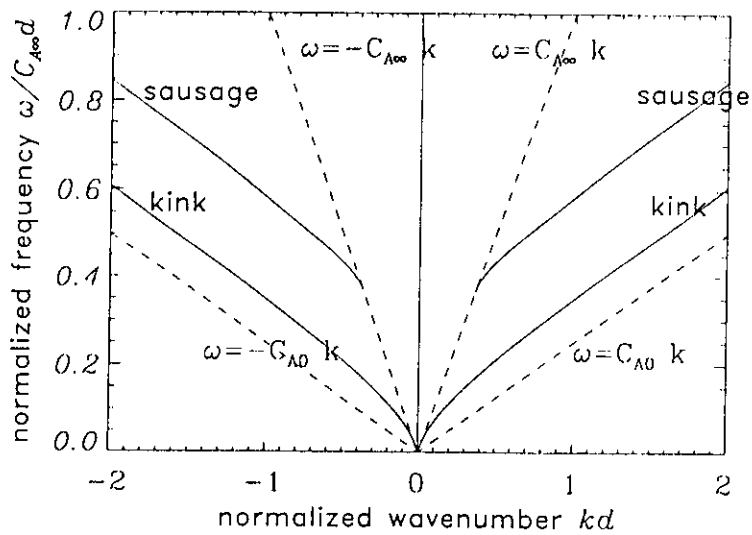


## 4.4 Alfvén wave phase mixing.

Alfvén waves are described by the equation

$$\left(\frac{\partial^2}{\partial t^2} - C_A^2(x)\frac{\partial^2}{\partial z^2}\right) V_y = 0, \tag{28}$$

with the solution

$$V_y = \Psi(x) f(z \mp C_A(x)t) \tag{29}$$

For a harmonic wave,

$$\left[\omega^2 - C_A^2(x)k_z^2\right] V_y = 0. \tag{30}$$

The structure of the Alfvèn wave in the transversal direction $x$ is an arbitrary function defined only by initial conditions.

$$k_z = \text{const}, k_x \to \infty. \tag{31}$$

This is the effect of Alfvén wave phase mixing (Heyvaerts & Priest 1983).

$$\text{Dissipation} = \nu \left( \frac{\partial^2}{\partial x^2} + \frac{\partial^2}{\partial z^2} \right) V_y$$

$$\propto \nu k_x^2.$$

*Enhanced dissipation.* In the developed stage of phase mixing:

$$V_y(z) = V_y(0) \exp \left\{ -\frac{\nu\omega^2}{6C_A^5(x)} \left[ \frac{\mathrm{d}C_A(x)}{\mathrm{d}x} \right]^2 z^3 \right\}. \tag{32}$$

$\nu$ is viscosity or resistivity, but both are very weak...

## 4.5 Resonant absorption.

When the phase speed of a wave coincides with one of the resonant speeds, $C_A(x)$ (Alfvén resonance) or $C_T(x)$ (cusp resonance), the wave can be subject to *resonant absorption.*

E.g.: Slab geometry, incompressible limit ($\gamma \to \infty$, $C_s \to \infty$). Alfvén and cusp resonances coincide. Consider a smooth magnetic interface:

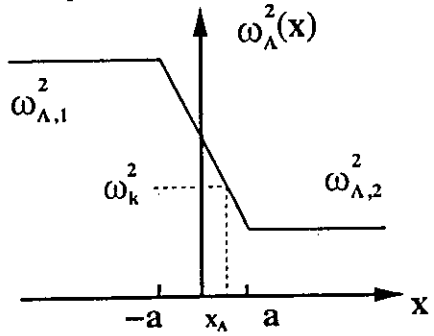

Governing equation for the transverse displacement is

$$\frac{\mathrm{d}}{\mathrm{d}x}\left[\rho_0(\omega^2-\omega_A^2)\frac{\mathrm{d}\xi}{\mathrm{d}x}\right]-(k_y^2+k_z^2)\rho_0(\omega^2-\omega_A^2)\xi=0, \tag{33}$$

where $\omega_A^2=(\mathbf{k}\dot{\mathbf{B}}_0)/(4\pi\rho_0)$.

Matching solutions of (33) in the homogeneous by the jump conditions:

$$[p_{\mathrm{total}}]=0 \quad \text{and} \quad \left[-i\pi\frac{\mathrm{sign}\omega}{\rho|\Delta|}(k_y^2+k_z^2)P_{\mathrm{total}}\right]=0,$$

we obtain the dispersion relation

$$\rho_1(\omega^2-\omega_{A1}^2)+\rho_2(\omega^2-\omega_{A2}^2)$$

$$-i\pi(k_y^2+k_z^2)^{1/2}\rho_1\rho_2\frac{(\omega^2-\omega_{A1}^2)(\omega^2-\omega_{A1}^2)}{(\rho|\Delta|)_{x_A}}=0, \tag{34}$$

where $\Delta=-\mathrm{d}\omega_A^2/\mathrm{d}x$ and $x_A$ is the position of the resonance.

$$\text{Damping coefficient} \quad \gamma=-\frac{\mathcal{D}_i(\omega_r,k)}{\partial\mathcal{D}_r/\partial\omega_r},$$

where $\mathcal{D}_i$ and $\mathcal{D}_r$ are the real and imaginary parts of the dispersion relation (c.f. Landau damping).

## 4.6 Effects of spherical stratification.

We consider a spherically stratified atmosphere permeated by a magnetic field:

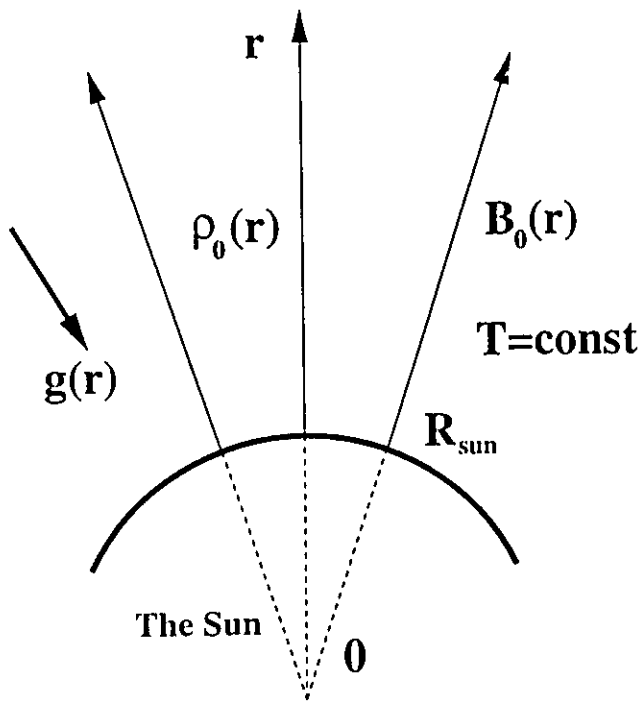


The magnetic field is strictly radial,

$$B_0(r) = \frac{B_0(R_\odot)R_\odot^2}{r^2}. \tag{35}$$

where $R_\odot$ is the solar radius and the gravitational acceleration is $g = GM_\odot/r^2$.

Assuming that the plasma is in hydrostatic equilibrium, we have for the density

$$\rho_0(r) = \rho_0(R_\odot) \exp\left(-\frac{R_\odot}{H}\frac{r - R_\odot}{r}\right), \tag{36}$$

where $H$ is the *scale height*, ($H$(Mm) $\approx$ 50T(MK)). From (35) and (36), the radial profile of the Alfvén speed $C_A$ is given by

$$C_A(r) = \frac{B_0(R_\odot)R_\odot^2}{r^2[4\pi\rho_0(R_\odot)]^{1/2}} \exp\left(\frac{R_\odot}{2H}\frac{r - R_\odot}{r}\right). \tag{37}$$

The atmosphere is assumed to be isothermal, with constant temperature $T$ and sound speed $C_s$ ($C_s$(Mm/s) = 0.152 $T^{1/2}$(MK)).

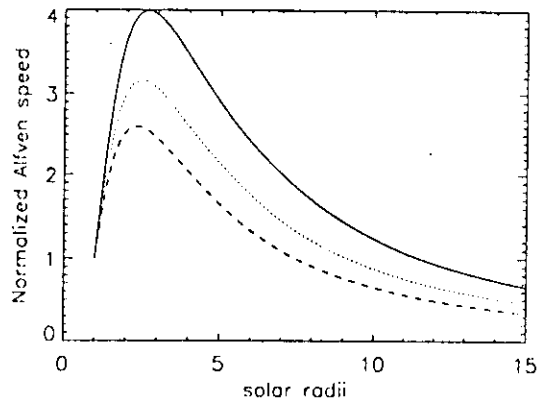

solid curve – T=1.3 MK, dotted – 1.4, dashed – 1.5

For purely radial propagation, we obtain two uncoupled *spherical* MHD modes,

the Alfvén wave (perturbes $B_\perp$ and $V_\perp$):

$$\frac{\partial^2 V_\phi}{\partial t^2} - \frac{B_0(r)}{4\pi\rho_0(r)r}\frac{\partial^2}{\partial r^2}\left[rB_0(r)V_\phi\right] = 0, \tag{38}$$

and slow magnetoacoustic wave (perturbes $\rho$ and $V_\parallel$):

$$\frac{\partial^2 \rho}{\partial t^2} - \frac{C_s^2}{r^2}\frac{\partial}{\partial r}\left(r^2\frac{\partial \rho}{\partial r}\right) - g\frac{\partial \rho}{\partial r} = 0.$$

Equations (38) and (4.6) can be solved in the WKB approximation (or the single wave approximation), $\epsilon = \lambda/H \ll 1$ and $H \ll R_\odot$.

## Alfvén Waves:

Following an upwardly propagating wave, and passing to the running frame of reference,

$$\tau = t - \int \frac{\mathrm{d}r}{C_A}, \qquad R = \epsilon r, \tag{39}$$

equation (38) is reduced to

$$\frac{\partial V_\phi}{\partial R} - \frac{R_\odot^2}{4H}\frac{1}{R^2}V_\phi = 0, \tag{40}$$

with the solution:

$$V_\phi = V_\phi(R_\odot) \exp\left(\frac{R - R_\odot}{4HR}\right). \tag{41}$$

The same result can be obtained by geometrical reasonings:

$$(\textbf{Poynting flux})_r = (\mathbf{B} \times \mathbf{V} \times \mathbf{B})_r \propto \frac{1}{r^2} \tag{42}$$

(an ideal linear spherical wave), on the other hand:

$$(\textbf{Poynting flux})_r \propto B_0 V_\phi B_\phi = V_\phi^2 B_0^2 / C_A \tag{43}$$

Consequently, $B_0 V_\phi^2 / C_A$ is constant, which gives us

$$V_\phi \propto [C_A(r)/B_0(r)]^{1/2} = \rho_0^{-1/4}(r), \tag{44}$$

which coincides with the dependence (41).

The relative Alfvén wave amplitude grows with height. Consequently, *nonlinear effects* come into play. Also, this is worth taking into account *dissipative* effects. Assuming that both the nonlinearity and viscosity are weak, we can add these effects to the evolutionary equation,

$$\frac{\partial V_\phi}{\partial R} - \frac{R_\odot^2}{4H}\frac{1}{R^2} V_\phi - \frac{1}{4C_A(C_A^2 - C_s^2)}\frac{\partial V_\phi^3}{\partial \tau} - \frac{\nu}{2C_A^3}\frac{\partial^2 V_\phi}{\partial \tau^2} = 0 \tag{45}$$

(see Nakariakov, Ofman & Arber 1999 for the rigorous derivation). Equation (45) is an analog of the *scalar Cohen-Kulsrud-Burgers equation* for the case of spherical geometry.

E.g.: Evolution of the shape of initially sinusoidal Alfvén wave with height,

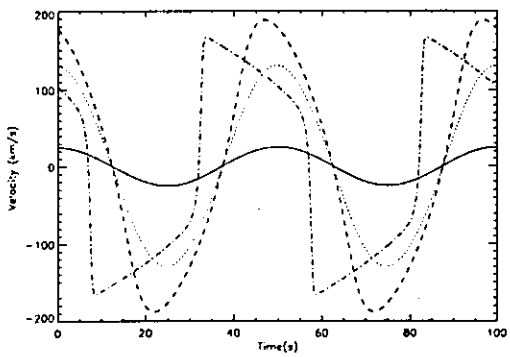

(The solid line corresponds to $R_\odot$, dotted to 2 $R_\odot$, dashed to 5 $R_\odot$, and dotted-dashed to 9 $R_\odot$.)

The wave grows, overturns and, consequently, is subject to nonlinear dissipation:

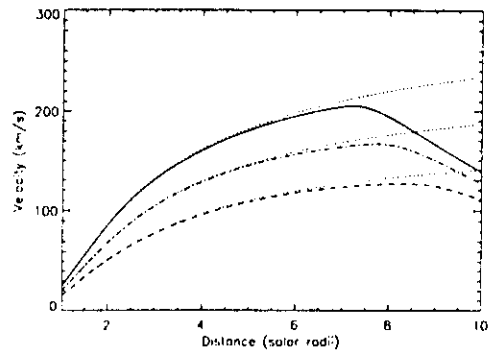


(The solid line corresponds to $A = 25$ km/s, the dash-dotted line to $A = 20$ km/s and the dashed line to $A = 15$ km/s. The dotted curves show the linear solution (41).)

The waves of shorter periods are subject to stronger nonlinear distortion and dissipation:

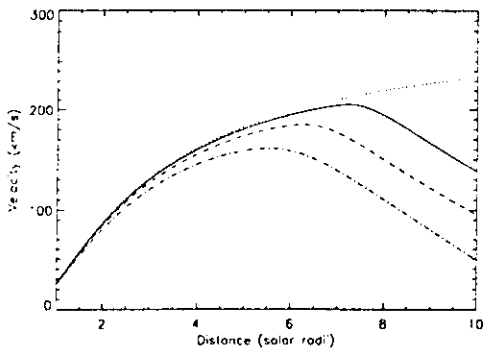


(The solid line corresponds to $P = 50$ s, the dashed line to $P = 25$ s and the dotted-dashed line to $P = 15$ s.)

Dependence of the breaking distance of an Alfvén wave upon the wave period:

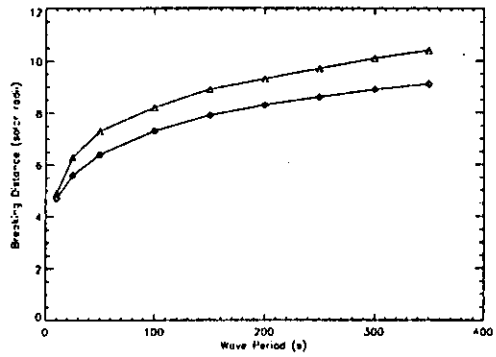


(The curve with triangles corresponds to the amplitude 25 km/s near the surface and with diamonds to 35 km/s. Temperature is 1.4 MK and the Alfvén speed is 1000 km/s near the base of the corona.)

## Slow Waves:

Similarly, we can process equation (4.6), taking into account nonlinearity and dissipation. Passing to the running frame of reference,

$$\xi = r - C_s t, \qquad R = \epsilon r, \tag{46}$$

we obtain

$$\frac{\partial \rho}{\partial R} + \left(\frac{1}{R} + \frac{g(R)}{2C_s^2}\right)\rho + \frac{1}{\rho_0(R)}\rho\frac{\partial \rho}{\partial \xi} - \frac{2\eta_0}{3C_s\rho_0(R)}\frac{\partial^2 \rho}{\partial \xi^2} = 0, \tag{47}$$

which is the *spherical Burgers equation* (see Ofman, Nakariakov & Sehgal 1999 for the detailed derivation) with the ideal linear solution

$$\rho = \rho(R_\odot)\frac{1}{R}\,\exp\left[-\frac{R_\odot}{2H}\left(1 - \frac{R_\odot}{R}\right)\right]. \tag{48}$$

The slow wave amplitude growths with heigh and becomes more and more nonlinear:

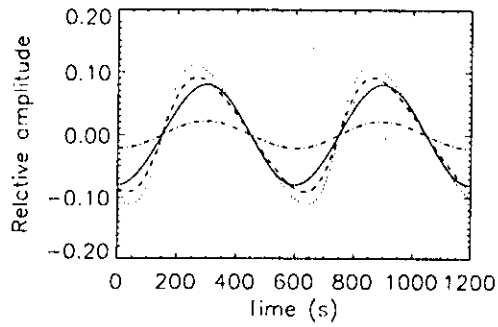


(The solid curve corresponds to the solution at $R = R_\odot$, dotted at $1.15R_\odot$, dashed to $1.3R_\odot$ and dash-dotted to $1.5R_\odot$. The initial wave amplitude is $A = 0.08$. The initial wave period is 600 s. The atmosphere is isothermal with $T = 1.4 \times 10^6$ K. The normalized viscosity is $\bar{\eta} = 3.2 \times 10^{-4}$.)

Thus, the slow wave is subject to nonlinear dissipation:

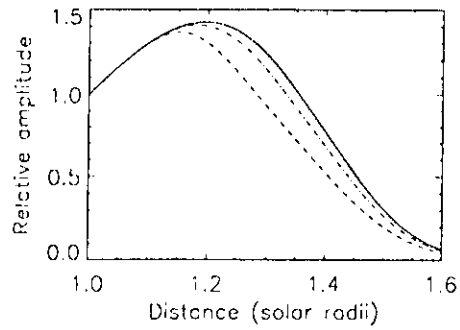


(The solid line corresponds to $A = 10^{-6}$, dotted line to $A = 0.02$, dash-dotted line to $A = 0.08$ and dashed line to $A = 0.16$.)

However, if the linear dissipation is sufficiently strong, the wave does not reach nonlinear effects:

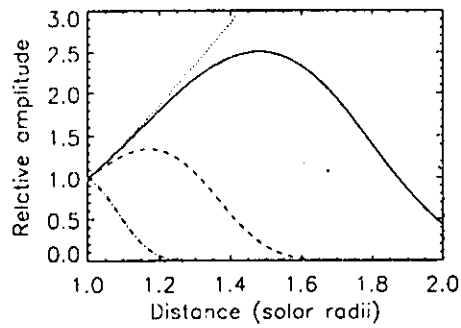


(The dotted line corresponds to $\bar{\eta} = \eta_0/C_s\rho_{00}R_\odot = 10^{-10}$, the solid line to $\bar{\eta} = 10^{-5}$, the dashed line to $\bar{\eta} = 10^{-4}$ and the dashed-dotted line to $\bar{\eta} = 10^{-3}$.)

Actually, the transport coefficients (viscosity, resistivity and thermal conduction) are unknown parameters.

## 4.7 Thin flux tube approximation

Consider a straight magnetic flux tube or slab of strength $B_0$ with cross-sectional area $A_0$, filled by a plasma of density $\rho_0$ and kinetic pressure $p_0$.

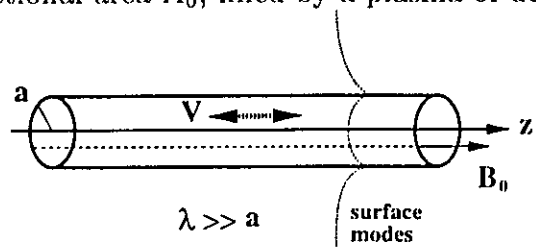


The dynamics of long wavelength waves may be described by the thin flux tube equations, viz.

$$\frac{\partial}{\partial t}\left(\frac{\rho}{B}\right) + \frac{\partial}{\partial z}\left(\frac{\rho v}{B}\right) = 0, \tag{49}$$

$$\frac{\partial v}{\partial t} + v\frac{\partial v}{\partial z} = -\frac{1}{\rho}\frac{\partial p}{\partial z}, \tag{50}$$

$$\frac{\partial p}{\partial t} + v\frac{\partial p}{\partial z} - \frac{\gamma p}{\rho}\left(\frac{\partial \rho}{\partial t} + v\frac{\partial \rho}{\partial z}\right) = 0, \tag{51}$$

$$p + \frac{B^2}{8\pi} = p_e. \tag{52}$$

Here $B(z,t)$ is the longitudinal component of the magnetic field, $v(z,t)$ the longitudinal component of the flow speed and $\rho(z,t)$ the plasma density. The plasma pressure $p(z,t)$ and magnetic pressure $B^2(z,t)/8\pi$ within the flux tube are in lateral balance with the surroundings at pressure $p_e(z,t)$, calculated on the external boundary of the tube. The cross-sectional area $A(z,t)$ of the tube can be calculated according to the invariant

$$BA = \text{constant}. \tag{53}$$

Equations (49)–(52) are an MHD analog of the shallow water theory. In particular, the equations are very convenient for consideration of nonlinear effects.

## 4.8 MHD solitons in magnetic structures.

Magnetoacoustic modes of plasma structures are subject to dispersion. In particular, long slow surface sausage waves are *weakly* dispersive. In the cylindric case, their phase speed is

$$V_p(k_z) \approx C_T - 2\Delta_T k_z^2 K_0(\lambda|k_z|), \tag{54}$$

where

$$\Delta_T = \frac{1}{8}\frac{\rho_e}{\rho_0}\frac{C_T^3(C_T^2 - C_{Ae}^2)}{C_A^4}a^2, \qquad \lambda^2 = \frac{(C_{se}^2 - C_T^2)(C_{Ae}^2 - C_T^2)}{(C_{se}^2 + C_{Ae}^2)(C_{Te}^2 - C_T^2)}a^2,$$

and the undisturbed tube is of radius $a$. In the case of the slab geometry,

$$V_p(k_z) \approx C_T - \Delta_s \pi |k_z|, \tag{55}$$

where

$$\Delta_s = \frac{1}{2\pi}\frac{\rho_e}{\rho_0}\left(\frac{C_T}{C_A}\right)^3 aC_T,$$

and the undisturbed slab is of width $2a$.

According to the dispersion laws, weakly nonlinear evolution of the waves is governed, in the cylindric case, by the Leibovich-Roberts (LR) equation, viz.

$$\frac{\partial v}{\partial t} + C_T \frac{\partial v}{\partial z} + \beta_{\rm nl} v \frac{\partial v}{\partial z} + \Delta_T \frac{\partial^3}{\partial z^3} \int_{-\infty}^{+\infty} \frac{v(z',t)\mathrm{d}z'}{[\lambda^2 + (z'-z)^2]^{1/2}} = 0, \qquad (56)$$

and, in the case of the slab geometry, by the Benjamin - Ono (BO) equation, viz.

$$\frac{\partial v}{\partial t} + C_T \frac{\partial v}{\partial z} + \beta_{\rm nl} v \frac{\partial v}{\partial z} + \Delta_s \frac{\partial^2}{\partial z^2} \int_{-\infty}^{+\infty} \frac{v(z',t)}{z'-z} \mathrm{d}z' = 0. \qquad (57)$$

The famous exact solution of the BO equation (57) is the algebraic soliton,

$$v(z,t) = \frac{A_{\rm sol}}{1 - [(z - V_{\rm sol})/L_{\rm sol}]^2}, \qquad (58)$$

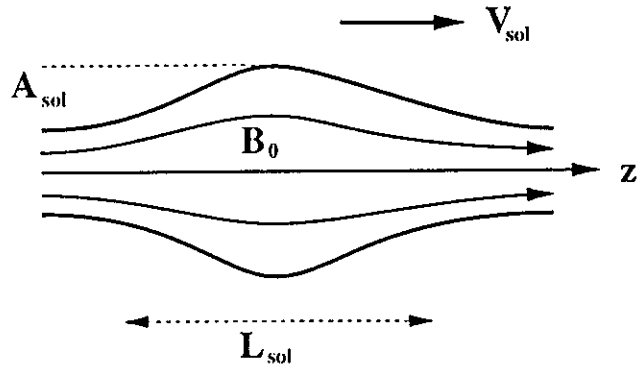


for amplitude $A_{\rm sol}$, length $L_{\rm sol}$ and speed $V_{\rm sol}$ related by

$$L_{\rm sol} = 4\Delta_s / A_{\rm sol}\beta_{\rm nl}, \quad V_{\rm sol} = C_T + A_{\rm sol}\beta_{\rm nl}/4. \qquad (59)$$

Exact solutions of the LR equation have not been found yet.

Ofman & Davila 1997, 1998 have numerically found solitary-like nonlinear MHD waves in coronal holes.

## 4.9 Nonlinear stage of phase mixing.

Consider nonlinear coupling of MHD waves on 1D inhomogeneity of a cold ($\beta = 0$) plasma.

For Alfvén waves (perturb $V_y$ and $B_y$ in the linear limit):

$$\frac{\partial^2}{\partial t^2} B_y - C_A^2(x) \frac{\partial^2}{\partial z^2} B_y =$$

$$\mathrm{N}_\mathrm{A}[B_x B_y]. \tag{60}$$

For fast magnetosonic waves (perturb $V_x$, $B_x$, $B_z$ and $\rho$ in the linear limit):

$$\frac{\partial^2}{\partial t^2} B_x - C_A^2(x) \left( \frac{\partial^2}{\partial x^2} + \frac{\partial^2}{\partial z^2} \right) B_x =$$

$$\mathrm{N}_\mathrm{FF}[B_x^2] + \mathrm{N}_\mathrm{FA}[B_y^2]. \tag{61}$$

where

$$\mathrm{N}_\mathrm{FA}[B_y^2] = \frac{B_0}{8\pi\rho_0(x)} \frac{\partial^2}{\partial x \partial z} B_y^2.$$

If $B_x(t=0) \ll B_y(t=0)$:

- Alfvén wave propagates as in the linear case
- Fast wave is excited by spatial gradients in the Alfvén wave

Let $B_y = f(z - C_A(x)t)$ (an initially plane wave),
$\Rightarrow$ For fast waves

$$\mathrm{RHS}(61) =$$

$$A^2 C_A^2(x) \frac{dC_A(x)}{dx} \left( f'(\xi) \int_0^t f''(\xi) t \, dt + t \, f''(\xi) \int_0^t f'(\xi) \, dt \right), \tag{62}$$

where $\xi = z - C_A(x)t$.

SECULAR GROWTH

If the profile of $C_A(x)$ contains a very sharp, but small change, we may take the Alfvén velocity as constant everywhere where it is not differentiated, and then

$$\left[\frac{\partial^2}{\partial t^2} - C_A^2\left(\frac{\partial^2}{\partial x^2} + \frac{\partial^2}{\partial z^2}\right)\right] V_x =$$

$$= C_A^2 A^2 \frac{dC_A(x)}{dx}\left(\frac{df}{d\xi}\int_0^t \frac{d^2 f}{d\xi^2} t\, dt + t\,\frac{d^2 f}{d\xi^2}\int_0^t \frac{df}{d\xi}\, dt\right). \qquad (63)$$

The forced solution of (63)

$$V_x(x,z,t) = \frac{1}{2\pi C_A}\int_0^t \int_\Sigma \int \frac{p(\bar{x},\bar{z},\tau)\, d\bar{x}\, d\bar{z}\, d\tau}{\left[C_A^2(t-\tau)^2 - (x-\bar{x})^2 - (z-\bar{z})^2\right]^{1/2}}, \qquad (64)$$

$\Sigma$ is the interior of the circle of radius $C_A(t-\tau)$ with centre at the point $p(x,z,t=0)$, with $p$ is RHS(63).

Thus, we have an *analytical* solution of a nonlinear MHD problem.

*Induced* longitudinal motions,

$$V_z = -\frac{1}{8\pi\rho_0(x)}\partial_t^{-1}\frac{\partial}{\partial z}B_y^2, \qquad (65)$$

do not grow secularly.

If the Alfvén wave is initially plane and harmonic,

$$V_y(x,z,t) = A\cos\Theta, \qquad \Theta = \omega\left(t - \frac{z}{C_A(x)}\right). \qquad (66)$$

$$\text{RHS(61)} =$$

$$\frac{\omega A^2}{C_A^2}\frac{dC_A(x)}{dx}\left[\omega z\cos\ 2\Theta - C_A(x)\sin 2\Theta\right]. \qquad (67)$$

Secular growth on the second harmonics.